Analytical potential formulae and fast algorithm for a horn torus resistor network

Zhaolin Jiang [1], Yufan Zhou [2,*], Xiaoyu Jiang [2,†] and Yanpeng Zheng [3]

[1] *School of Mathematics and Statistics, Linyi University, Linyi 276000, People's Republic of China*

[2] *School of Information Science and Engineering, Linyi University, Linyi 276000, People's Republic of China*

[3] *School of Automation and Electrical Engineering, Linyi University, Linyi 276000, People's Republic of China*

(Received 24 November 2022; accepted 4 April 2023; published 25 April 2023)

In this paper, a $(u+1)\times v$ horn torus resistor network with a special boundary is researched. According to Kirchhoff's law and the recursion-transform method, a model of the resistor network is established by the voltage V and a perturbed tridiagonal Toeplitz matrix. We obtain the exact potential formula of a horn torus resistor network. First, the orthogonal matrix transformation is constructed to obtain the eigenvalues and eigenvectors of this perturbed tridiagonal Toeplitz matrix; second, the solution of the node voltage is given by using the famous fifth kind of discrete sine transform (DST-V). We introduce Chebyshev polynomials to represent the exact potential formula. In addition, the equivalent resistance formulae in special cases are given and displayed by a three-dimensional dynamic view. Finally, a fast algorithm of computing potential is proposed by using the mathematical model, famous DST-V, and fast matrix-vector multiplication. The exact potential formula and the proposed fast algorithm realize large-scale fast and efficient operation for a $(u+1)\times v$ horn torus resistor network, respectively.

DOI: 10.1103/PhysRevE.107.044123

I. INTRODUCTION

The resistor network model has a wide range of applications and plays an important role in physics and material science. In 2010, in particular, the Nobel Prize in Physics was awarded to the discoverer of the graphene network, which not only proved that resistive networks exist in reality, but also that they are of great value. In 2018, Hadad *et al.* [1] established a model based on the work of Su, Schrieffer, and Heeger, using a dimer circuit to achieve self-induced topological protection in nonlinear circuit arrays. In 2021, Zhang *et al.* [2] studied an ERCM (enhanced reliability centered maintenance) technology by establishing a resistor network model and applied a resistance change method to material damage detection for CFRPs (carbon fiber reinforced plastics) panels damage location and pattern recognition. In the past few years, many results have been achieved in the study of resistor networks [3–15] and neural networks [16–22]. Since Kirchhoff [3] established the basic circuit theory (node current law and circuit voltage law) in 1845, the resistor network starts to develop. In afterward research, Cserti [9] studied Green's function technology to solve the equivalent resistance problem of the infinite network. Until 2004, Wu [10] put forward the Laplacian matrix method of the resistor network. Shi *et al.* [16,17] studied a discrete-time recurrent neural network. Liu *et al.* [18] and Sun *et al.* [19] proposed different types of the zeroing neural network. And Jin *et al.* [20–22] studied an innovative control theory stimulated gradient neural network algorithm.

In the following research, researchers found several effective methods to solve the effective resistance of resistor networks with different structures, but the potential formula of complex networks is still an unsolved problem. In 2011, Tan [23] established an advanced resistance network model recursion-transform (RT) theory. After 2014, Tan made breakthroughs and proposed some network models (globe network, fan network, etc.). With the development of RT theory, it is divided into two methods: one is to establish the matrix equations model based on current parameters (RT-I) and the other is to establish the matrix equations model based on voltage parameters (RT-V). Tan [24] proposed an accurate potential formula for solving arbitrary cobweb and fan networks using voltage parameters (RT-V). After that, Z. Tan *et al.* [25] found a nonregular fan network with any two boundaries and many interesting networks SNAIL (simple neural attention meta-learner) network and HART (highway addressable remote transducer) network were obtained with different boundary conditions. Since then, many achievements have been made [26–33]. In 2020, Tan *et al.* [31] published the basic principles of resistive networks and made breakthroughs, which can be applied to various types of network structures and solve the analytical solutions of complex networks, such as the nonregular cylindrical network. In the same year, Tan *et al.* [32] studied the network models of cylindrical networks with arbitrary boundaries, including cobweb network, globe network, and other multiple topologies. In 2021, Chen *et al.* [33] proposed a complex impedance network model of two terminal ladder networks and deduced the analytic formula of its equivalent complex impedance of the n-order RLC network. The above literature shows that much research is based on RT methods to achieve breakthrough progress. The RT method requires the use of a tridiagonal matrix to construct

*Corresponding author: zyf19970201@sina.com

†jxy19890422@sina.com

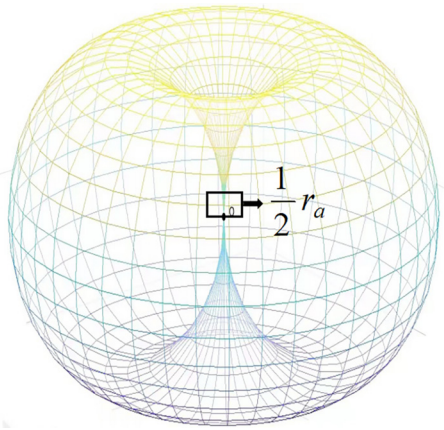

FIG. 1. $(u+1)\times v$ horn torus network with $(u+1)$ horizontal and v vertical grids and its horizontal resistances are r_b. There are u latitude lines, v longitude lines, and a zero potential point O. Let Y_k denote an arbitrary node along the longitude and the resistances between Y_u and O are $\frac{1}{2}r_a$, while the resistances at all other nodes along the longitude are r_a.

a mathematical model and the eigenvalues of this matrix must be used to express the exact potential formula. At present, there have been many results on tridiagonal matrices [34–40], which are also widely used. It can be said that it is a powerful tool to solve the problem of the resistor network [24,41–51]. The structure of things in the real world is diverse and very complex and network models are also developing in a diversified way. New network models need to be excavated.

The rest of this paper is organized as follows. In Sec. II, the exact potential formulae of a $(u+1)\times v$ horn torus resistor network are given. In Sec. III, the detailed derivation process of the exact potential formula is introduced. In Sec. IV, some special cases of potential formula are discussed and displayed by a three-dimensional (3D) dynamic view. In Sec. V, a fast algorithm of computing potential is proposed by using the mathematical model, famous DST-V, and fast matrix-vector multiplication. Finally, the paper is summarized in Sec. VI.

II. EXACT POTENTIAL FORMULAE

In this section, we will give the exact potential formula of the horn torus resistor network and give a potential formula of the infinite network. Through the 3D dynamic view, we will show the whole process of the changing graph for the potential with the current input and output point change.

A $(u+1)\times v$ horn torus resistor network is proposed, of which $u+1$ and v are the numbers of grids along latitude and longitude directions as shown in Fig. 1 and its horizontal resistances are r_b. There are u latitude lines, v longitude lines, and a zero potential point O. Y_k denotes an arbitrary node along the longitude and the resistances between Y_u and O are $\frac{1}{2}r_a$, while the resistances at all other nodes along the longitude are r_a. Set the potential of O point to zero, the U/J axis is taken as Y, and the coordinates $\{x, y\}$ represent the nodes of the network. The current J flows in from $d_1(x_1, y_1)$ and flows out from $d_2(x_2, y_2)$. For the convenience of expression, we abbreviate $U_{(u+1)\times v(x,y)}/J$ as $U_{u\times v}(x, y)/J$ and the potential of any node of any horn torus resistor network can be expressed

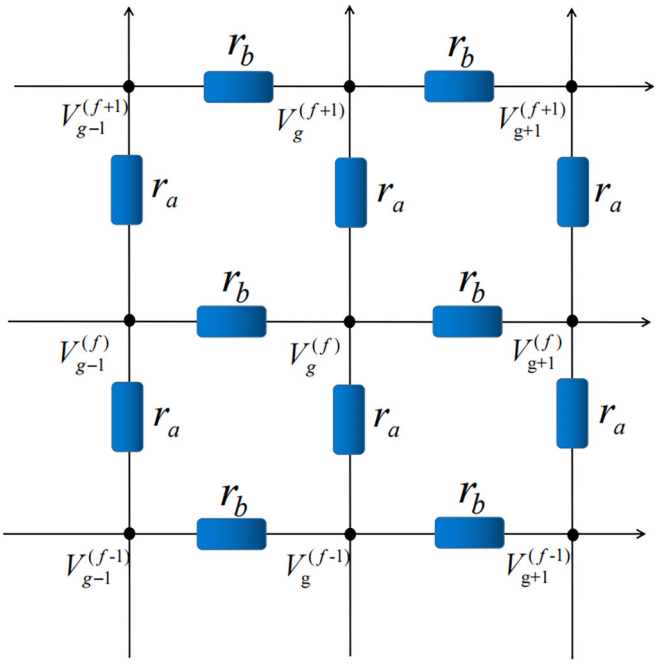

FIG. 2. Segment of the horn torus resistor network with potential parameters.

as follows:

$$\frac{U_{u\times v}(x,y)}{J} = \frac{4r_b}{2u+1}\sum_{f=1}^{u}\mathcal{A}_f, \tag{1}$$

where

$$\mathcal{A}_f = \left(\frac{\varpi_{x_1,x}^{(f)}K_{y_1,f} - \varpi_{x_2,x}^{(f)}K_{y_2,f}}{G_{v+1}^{(f)} - G_{v-1}^{(f)} - 2}\right)K_{y,f},$$

$$\varpi_{x_m,x}^{(f)} = G_{v-|x_m-x|}^{(f)} + G_{|x_m-x|}^{(f)}, \quad m = 1, 2, \tag{2}$$

$$G_g^{(f)}(\cosh\varphi_f) = \frac{\sinh(g\varphi_f)}{\sinh(\varphi_f)}, \quad \cosh\varphi_f = \iota_f/2, \quad \varphi_f > 0, \tag{3}$$

$$g = v-|x_1-x|, |x_1-x|, v-|x_2-x|, |x_2-x|, \ v+1, v-1,$$
$$f = 1, 2, \ldots, u,$$

$$K_{q,f} = \sin\frac{2qf\pi}{2u+1}, \quad q = y_1, y_2, y, \tag{4}$$

$$\iota_f = 2 + \frac{2r_b}{r_a} - \frac{2r_b}{r_a}\cos\frac{2f\pi}{2u+1}. \tag{5}$$

In particular, the input and output points can be one or more, so formula (1) applies to all coordinate points (x_g, y_g) $(0 \leqslant g \leqslant v)$. Therefore, q can also be $y_3, y_4, \ldots, y_g$.

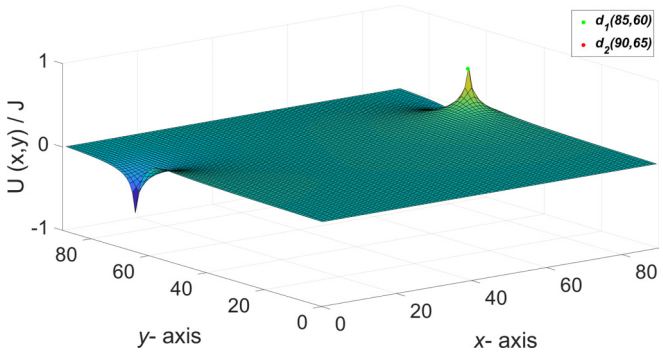

FIG. 3. 3D view for $U_{90\times 90}(x, y)/J$ with the current input and output point.

When Fig. 2 is a semi-infinite network, the nodal potential in the horn torus resistor network is denoted by

$$\frac{U_{u\times\infty}(x, y)}{J} = \frac{8r_b}{2u+1}\sum_{f=1}^{u}\sinh(\varphi_f)\mathcal{B}_f K_{y,f}, \tag{6}$$

where

$$\mathcal{B}_f = \left(\frac{\left(e^{-|x_1-x|\varphi_f}K_{y_1,f} - e^{-|x_2-x|\varphi_f}K_{y_2,f}\right)}{\iota_f^2 - 4}\right).$$

φ_f, $K_{q,f}$, and ι_f are the same as Eqs. (3), (4), and (5), respectively. Formula (6) is the potential formula for any point $d(x, y)$ in the horn torus resistor network.

Remark. Based on formula (1) of the resistor network, as shown in Fig. 3, we dynamically displayed the changing graph of the potential with the current input point $[d_1(x_1, y_1)]$ and output point $[d_2(x_2, y_2)]$ change, which can more intuitively feel the whole change process through the image, providing a dynamic visualization case analysis for the research of the resistor network.

III. DERIVATION OF POTENTIAL FORMULA

A. Overall idea and design

So as to calculate the potential of the nodes in the horn torus resistor network, assume that the current J goes from $d_1(x_1, y_1)$ input to $d_2(x_2, y_2)$ output. Figure 2 shows the voltages of the resistor network. All the voltages in the horizontal direction are represented as $V_1^{(f)}, V_2^{(f)}, \ldots, V_v^{(f)}$ $(0 \leqslant f \leqslant u)$, where the resistance is r_b, and all the voltages in the vertical direction are represented as $V_g^{(1)}, V_g^{(2)}, \ldots, V_g^{(u)} (0 \leqslant g \leqslant v)$, where the resistance is r_a.

Suppose that the potential of O points to zero; then calculating the node potential between any two points can be described as

$$U_{u\times v}(x, y) = V_x^{(y)} - 0 = V_x^{(y)}, \tag{7}$$

where $V_x^{(y)}$ is denoted by voltage.

B. Modeling on account of Kirchhoff's law and a perturbed tridiagonal Toeplitz matrix

The establishment of the network model is essential, so in this section we will model the network through the analysis of the network and give the boundary equations.

First of all, we cut off a partial resistor network as shown in Fig. 2. Applying Kirchhoff's law, the recurrence relation equations of node potential are obtained as follows:

$$\begin{aligned}
&V_{g+1}^{(1)} = (2+2\sigma)V_g^{(1)} - \sigma V_g^{(2)} - V_{g-1}^{(1)},\\
&\quad f = 1, \quad 0 \leqslant g \leqslant v,\\
&V_{g+1}^{(f)} = (2+2\sigma)V_g^{(f)} - \sigma V_g^{(f-1)} - \sigma V_g^{(f+1)} - V_{g-1}^{(f)},\\
&\quad 1 < f < u, \quad 0 \leqslant g \leqslant v,\\
&V_{g+1}^{(u)} = (2+3\sigma)V_g^{(u)} - \sigma V_g^{(u-1)} - V_{g-1}^{(u)},\\
&\quad f = u, \quad 0 \leqslant g \leqslant v,
\end{aligned} \tag{8}$$

where $\sigma = r_b/r_a$. By Eq. (8), we get a general matrix equation

$$\mathbf{V}_{g+1} = \mathbf{Q}_u\mathbf{V}_g - \mathbf{V}_{g-1} - r\mathbf{I}_g, \tag{9}$$

where V_g and I_g are the $u \times 1$ column matrices separately and can be described by

$$\mathbf{V}_g = \left[V_g^{(1)}, V_g^{(2)}, V_g^{(3)}, \ldots, V_g^{(u)}\right]^T \quad (0 \leqslant g \leqslant v), \tag{10}$$

$$I_g = J(\xi_{y_1,g} - \xi_{y_2,g}), \tag{11}$$

the function $\xi_{y,g}$ is defined as $\xi_{y,g}(y = g) = 1, \xi_{g,y}(y \neq g) = 0$, the matrix Q_u is a $u \times u$ perturbed tridiagonal Toeplitz matrix,

$$\mathbf{Q}_u = \begin{bmatrix}
2+2\sigma & -\sigma & 0 & \cdots & \cdots & 0\\
-\sigma & 2+2\sigma & -\sigma & \ddots & & \vdots\\
0 & -\sigma & \ddots & \ddots & \ddots & \vdots\\
\vdots & \ddots & \ddots & \ddots & -\sigma & 0\\
\vdots & & \ddots & -\sigma & 2+2\sigma & -\sigma\\
0 & \cdots & \cdots & 0 & -\sigma & 2+3\sigma
\end{bmatrix}_{u\times u}, \tag{12}$$

and $\sigma = r_b/r_a$. The matrix equation model of a $(u+1) \times v$ horn torus resistor network is Eq. (9).

Secondly, in light of the RT-V method, we need to apply Kirchhoff's law to establish boundary condition equations by the left and right edges,

$$\mathbf{V}_{v-1} + \mathbf{V}_1 = \mathbf{Q}_u\mathbf{V}_0 \tag{13}$$

and

$$\mathbf{V}_0 = \mathbf{V}_v = \mathbf{Q}_u\mathbf{V}_{v-1} - \mathbf{V}_{v-2}, \tag{14}$$

where matrix $\mathbf{Q}_u$ is given by Eq. (12). Owing to its periodicity, $\mathbf{V}_0 = \mathbf{V}_v$.

The potential formula (1) we need is obtained by Eqs. (9), (10), (11), (12), (13), and (14), but Eq. (9) is an extremely complex matrix equation, which cannot be directly solved by using ordinary methods.

C. Horadam sequence and the orthogonal diagonalization of the matrix $\mathbf{Q}_u$

In this section, in order to improve the actual performance and realize the fast algorithm for computing the potential, we introduce the famous Horadam sequence represented by the Chebyshev polynomial of the second kind and the fifth kind of discrete sine transformation.

Different from the RT method, we use the Chebyshev polynomials of the second kind to denote the Horadam sequence. The Horadam sequence is defined by the following conditions:

$$W_g = dW_{g-1} - qW_{g-2}, \quad W_0 = a, \quad W_1 = b, \tag{15}$$

where $g \in \mathbf{N}$, $g \geqslant 2$, $a, b, d, q \in \mathbf{C}$, $\mathbf{N}$ is the set of all natural numbers, and $\mathbf{C}$ is the set of all complex numbers.

We know that the Horadam sequence [52] represented by Chebyshev polynomials of the second kind is

$$W_g = (\sqrt{q})^g \left[\frac{b}{\sqrt{q}} U_{g-1}\left(\frac{d}{2\sqrt{q}}\right) - aU_{g-2}\left(\frac{d}{2\sqrt{q}}\right)\right],$$

where

$$U_g(\cos\varphi) = \frac{\sin(g+1)\varphi}{\sin\varphi}, \quad \cos\varphi = \frac{d}{2\sqrt{q}}, \quad \varphi \in \mathbf{C} \tag{16}$$

are the Chebyshev polynomials of the second kind [53].

In physics, we need to convert to a real number field. Since Eq. (16) is a representation in the complex number field, the representation in the real number field is as follows:

$$U_g(\cosh\varphi) = \frac{\sinh(g+1)\varphi}{\sinh\varphi}, \quad \cosh\varphi = \frac{d}{2\sqrt{q}}, \quad \varphi \in \mathbf{R}.$$

If we put $q = 1$, $d = \iota_f$, a, and b, in (15), we obtain the sequence $(R_g^{(f)})_{g\geqslant 0}$, where

$$R_g^{(f)} = bU_{g-1}^{(f)}\left(\frac{\iota_f}{2}\right) - aU_{g-2}^{(f)}\left(\frac{\iota_f}{2}\right), \tag{17}$$

$$U_g^{(f)}(\cosh\varphi_f) = \frac{\sinh(g+1)\varphi_f}{\sinh\varphi_f}.$$

φ_f and ι_f are given in Eqs. (3) and Eqs. (5), respectively.

In order to obtain an analytical solution of the potential and a fast numerical algorithm for computing the potential, let us first give the orthogonal diagonalization of the matrix $\mathbf{Q}_u$.

Q_u is given in Eq. (12). Then the eigenvalues $\iota_1, \ldots, \iota_u$ of $\mathbf{Q}_u$ are given by

$$\iota_f = 2 + \frac{2r_b}{r_a} - \frac{2r_b}{r_a}\cos\frac{2f\pi}{2u+1} \tag{18}$$

and the corresponding eigenvectors $\omega^{(f)} = (\omega_1^{(f)}, \ldots, \omega_u^{(f)})^\dagger$ are given by

$$\omega_v^{(f)} = \frac{2}{\sqrt{2u+1}}\sin\frac{2vf\pi}{2u+1}, \quad v = 1, 2, \ldots, u, \quad f = 1, 2, \ldots, u. \tag{19}$$

Let

$$\mathbf{S}_u^V = \frac{2}{\sqrt{2u+1}}\left(\sin\frac{2fv\pi}{2u+1}\right)_{v,f=1}^{u}.$$

Clearly, the matrix $\mathbf{S}_u^V$ is the famous fifth kind of discrete sine transform (DST-V) [54–56]. $\mathbf{S}_u^V$ is an orthogonal matrix and the inverse of $\mathbf{S}_u^V$ is actually $\mathbf{S}_u^V$, i.e.,

$$\left(\mathbf{S}_u^V\right)^{-1} = \left(\mathbf{S}_u^V\right)^T = \mathbf{S}_u^V. \tag{20}$$

By calculation we obtain the orthogonal diagonalization of the matrix $\mathbf{Q}_u$ as follows:

$$\left(\mathbf{S}_u^V\right)^{-1}\mathbf{Q}_u\left(\mathbf{S}_u^V\right) = \mathrm{diag}(\iota_1, \iota_2, \ldots, \iota_u), \tag{21}$$

i.e.,

$$\mathbf{Q}_u = \left(\mathbf{S}_u^V\right)\mathrm{diag}(\iota_1, \iota_2, \ldots, \iota_u)\left(\mathbf{S}_u^V\right)^{-1}.$$

According to Eq. (21), the eigenvalues ι_f, $f = 1, 2, \ldots, u$ in Eq. (18) and the eigenvectors $\omega^{(f)} = (\omega_1^{(f)}, \ldots, \omega_u^{(f)})^\dagger$ in Eq. (19) are obtained, respectively.

D. Orthogonal matrix transform method

In this section, we solve Eq. (9) by orthogonal matrix transformation. First, we multiply the left side of Eq. (9) by an orthogonal matrix $\mathbf{S}_u^V$, which is the fifth kind of discrete sine transformation matrix, and we obtain

$$\mathbf{S}_u^V\mathbf{V}_{g+1} = \mathbf{S}_u^V\mathbf{Q}_u\mathbf{V}_g - \mathbf{S}_u^V\mathbf{V}_{g-1} - r\mathbf{S}_u^V\mathbf{I}_g. \tag{22}$$

By Eqs. (20) and (21), we have

$$\mathbf{S}_u^V\mathbf{Q}_u = \mathbf{T}_u\mathbf{S}_u^V, \tag{23}$$

where $T_u = \mathrm{diag}(\iota_1, \iota_2, \ldots, \iota_u)$.

By Eqs. (22) and (23), we have

$$\mathbf{S}_u^V\mathbf{V}_g = \mathbf{R}_g, \quad \mathbf{V}_g = \mathbf{S}_u^V\mathbf{R}_g, \tag{24}$$

where $\mathbf{R}_g$ is the $u \times 1$ column vector, i.e.,

$$\mathbf{R}_g = \left[R_g^{(1)}, R_g^{(2)}, \ldots, R_g^{(u)}\right]^T \quad (0 \leqslant g \leqslant v). \tag{25}$$

Combining Eqs. (23) and (24) with Eq. (22), we have the following equation:

$$R_{g+1}^{(f)} = \iota_f R_g^{(f)} - R_{g-1}^{(f)} - rJ\varepsilon_{y,f}, \tag{26}$$

where

$$\varepsilon_{1,f} = \frac{2}{\sqrt{2u+1}}\sin\left(\frac{2y_1 f\pi}{2u+1}\right), \quad \varepsilon_{2,f} = -\frac{2}{\sqrt{2u+1}}\sin\left(\frac{2y_2 f\pi}{2u+1}\right). \tag{27}$$

After that, multiplying Eqs. (13) and (14) from the left-hand side by matrix $\mathbf{S}_u^V$, the following equations are derived:

$$R_{v-1}^{(f)} + R_1^{(f)} = \iota_f R_0^{(f)} \tag{28}$$

and

$$R_0^{(f)} = R_v^{(f)} = \iota_f R_{v-1}^{(f)} - R_{v-2}^{(f)}. \tag{29}$$

E. Analytical solution of matrix equation expressed by Chebyshev polynomials

In this section, let $G_g^{(f)} = U_{g-1}^{(f)}$. By Eqs. (26), (28), (29), and (17), the exact solution of $R_g^{(f)}$ will be derived. Presuming that the current J is input from $d_1(x_1, y_1)$ and output from

$d_2(x_2, y_2)$, the piecewise solution is obtained from formula (26):

$$R_g^{(f)} = R_1^{(f)} G_g^{(f)} - R_0^{(f)} G_{g-1}^{(f)}, \quad 0 \leqslant g \leqslant x_1, \tag{30}$$

$$R_{x_1+1}^{(f)} = \iota_f R_{x_1}^{(f)} - R_{x_1-1}^{(f)} - rJ\varepsilon_{1,f}, \tag{31}$$

$$R_g^{(f)} = R_{x_1+1}^{(f)} G_{g-x_1}^{(f)} - R_{x_1}^{(f)} G_{g-x_1-1}^{(f)}, \quad x_1 \leqslant g \leqslant x_2, \tag{32}$$

$$R_{x_2+1}^{(f)} = \iota_f R_{x_2}^{(f)} - R_{x_2-1}^{(f)} - rJ\varepsilon_{2,f}, \tag{33}$$

$$R_g^{(f)} = R_{x_2+1}^{(f)} G_{g-x_2}^{(f)} - R_{x_2}^{(f)} G_{g-x_2-1}^{(f)}, \quad x_2 \leqslant g \leqslant v, \tag{34}$$

where $G_g^{(f)}$ has been defined in Eq. (3).

By solving Eqs. (28), (29), (30), (31), (32), (33), and (34), the general solution of $R_g^{(f)}$ is obtained as follows:

$$R_x^{(f)} = r_b J \frac{\varpi_{x_1,x}^{(f)} \varepsilon_{1,f} + \varpi_{x_2,x}^{(f)} \varepsilon_{2,f}}{G_{v+1}^{(f)} - G_{v-1}^{(f)} - 2}, \quad 0 \leqslant x \leqslant v, \quad 1 \leqslant f \leqslant u, \tag{35}$$

where $\varpi_{x_m,x}^{(f)}$, $\varepsilon_{1,f}$, $\varepsilon_{2,f}$, and $G_g^{(f)}$ are given by Eqs. (2), (27), and (3), respectively.

The above results in a complicated expression $R_g^{(f)}$ composed of three piecewise functions. According to the general solution Eq. (35), we can calculate the branch voltage and node potential.

F. Derivation of an analytical formula for the potential

In this section, we will deduce the final potential formula and discuss interesting formulae for finite or infinite conditions. Above all, we use the general solution of $R_g^{(f)}$ to calculate the node potential. The node voltage $V_g^{(f)}$ is gained by means of Eq. (24):

$$V_x^{(y)} = \frac{2}{\sqrt{2u+1}} \sum_{f=1}^{u} \sin\left(\frac{2yf\pi}{2u+1}\right) R_x^{(f)}. \tag{36}$$

By Eqs. (35) and (36), we have

$$V_x^{(y)} = \frac{2r_b J}{\sqrt{2u+1}} \sum_{f=1}^{u} \mathcal{D}_f, \tag{37}$$

where

$$\mathcal{D}_f = \left(\frac{\varpi_{x_1,x}^{(f)} \varepsilon_{1,f} + \varpi_{x_2,x}^{(f)} \varepsilon_{2,f}}{G_{v+1}^{(f)} - G_{v-1}^{(f)} - 2}\right) \sin\left(\frac{2yf\pi}{2u+1}\right),$$

$\varpi_{x_m,x}^{(f)}$, $G_g^{(f)}$, $\varepsilon_{1,f}$, and $\varepsilon_{2,f}$ are defined in Eqs. (2), (3), and (27), respectively.

Furthermore, when v tends to infinity but u is finite, the following formula will be obtained by means of Eqs. (3) and (5):

$$\lim_{v\to\infty} \frac{G_{v-|g-x|}^{(f)} + G_{|g-x|}^{(f)}}{G_{v+1}^{(f)} - G_{v-1}^{(f)} - 2} = 2\sinh(\varphi_f) \frac{e^{-|g-x|\varphi_f}}{\iota_f^2 - 4}, \tag{38}$$

where φ_f and ι_f are the same as Eqs. (3) and (5).

By Eqs. (38) and (37), we obtain

$$\frac{U_{u\times\infty}(x,y)}{J} = \frac{4r_b}{\sqrt{2u+1}} \sum_{f=1}^{u} \mathcal{E}_f \sin\frac{2yf\pi}{2u+1}, \tag{39}$$

where

$$\mathcal{E}_f = \left(\frac{(e^{-|x_1-x|\varphi_f}\varepsilon_{1,f} + e^{-|x_2-x|\varphi_f}\varepsilon_{2,f})\sinh(\varphi_f)}{\iota_f^2 - 4}\right).$$

$\varepsilon_{1,f}$, $\varepsilon_{2,f}$ and ι_f are given by Eqs. (27) and (5), respectively. By Eqs. (27) and (39), we obtain Eq. (6).

Up to now, by bringing formula (27) into formula (37), formula (1) is obtained. Two general potential formulae (1) and (6) of a $(u+1)\times v$ horn torus resistor network have been proved.

IV. SEVERAL CASES OF INTERESTING FORMS FOR POTENTIAL FORMULAE

Since formula (1) is a general potential conclusion of a horn torus resistor network includes all cases. If taking some special conditions in formula (1), then we get a series of fascinating results under various parameters. The environment of special cases is carried out in a $(u+1)\times v$ horn torus resistor network as shown in Fig. 1. Presuming that $O = 0$ is the origin, the current J input at the node $d_1(x_1, y_1)$ and exit at the node $d_2(x_1, y_2)$.

Case 1. Suppose the current J flows in from the origin $O = 0$ and out from $d(x, y)$; the potential of any two points can be written as

$$\frac{U_{u\times v}(x,y)}{J} = \frac{4r_b}{2u+1} \sum_{f=1}^{u} \left(\frac{\varpi_{x_1,x}^{(f)} K_{y_1,f} K_{y,f}}{G_{v+1}^{(f)} - G_{v-1}^{(f)} - 2}\right),$$

where $\varpi_{x_1,x}^{(f)}$, $G_g^{(f)}$, and $K_{q,f}$ are the same as Eqs. (2), (3), and (4), respectively.

When $u = v = 90$, $x_1 = y_1 = 40$, $x_2 = y_2 = 0$, and $r_a = r_b = 1$, the following formula is obtained:

$$\frac{U_{90\times 90}(x,y)}{J} = \frac{4}{181} \sum_{f=1}^{90} \mathcal{G}_f, \tag{40}$$

where

$$\mathcal{G}_f = \left(\frac{\sin\left(\frac{80f\pi}{181}\right)\sin\frac{2yf\pi}{181}}{G_{91}^{(f)} - 2G_{89}^{(f)} - 2}\right)\varpi_{40,x}^{(f)}, \tag{41}$$

$$\varpi_{40,x}^{(f)} = \left(G_{90-|40-x|}^{(f)} + G_{|40-x|}^{(f)}\right),$$

$$G_g^{(f)}(\cosh\varphi_f) = \frac{\sinh(g\varphi_f)}{\sinh\varphi_f}, \quad \cosh\varphi_f = \left(2 - \cos\frac{2f\pi}{181}\right), \tag{42}$$

$$g = 90 - |40 - x|, |40 - x|, 91, 89, \quad f = 1, 2, \ldots, 90.$$

The 3D view is shown in Fig. 4 by MATLAB.

Case 2. Presume that when the current J is injected at node $d_1(x_1, y_1)$ and the current J is withdrawn at node $d_2(x_1, y_2)$, the potential of any node $d(x, y)$ is

$$\frac{U_{u\times v}(x,y)}{J} = \frac{4r_b}{2u+1} \sum_{f=1}^{u} \mathcal{H}_f K_{y,f},$$

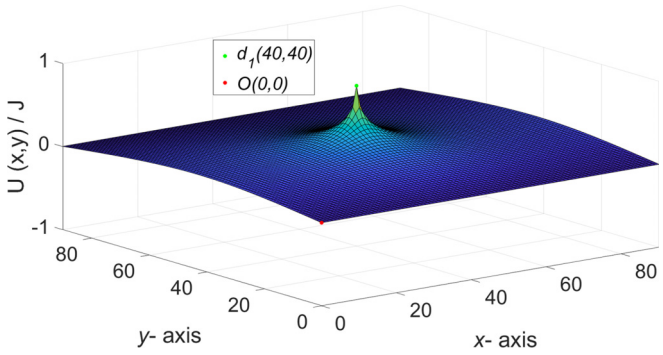

FIG. 4. 3D view for the $U_{90\times90}(x, y)/J$ in Eq. (40).

where

$$\mathcal{H}_f = \left(\frac{(K_{y_1,f} - K_{y_2,f})\varpi_{x_1,x}^{(f)}}{G_{v+1}^{(f)} - G_{v-1}^{(f)} - 2}\right),$$

and $\varpi_{x_1,x}^{(f)}$, $G_g^{(f)}$, and $K_{q,f}$ are defined in Eqs. (2), (3), and (4), respectively.

When $u = v = 90$, $x_1 = x_2 = y_1 = 40$, $y_2 = 30$, and $r_a = r_b = 1$, the following formula is gained:

$$\frac{U_{90\times90}(x, y)}{J} = \frac{4}{181}\sum_{f=1}^{90}\mathcal{I}_f \sin\frac{2yf\pi}{181}, \tag{43}$$

where

$$\mathcal{I}_f = \left(\frac{\left[\sin\left(\frac{80f\pi}{181}\right) - \sin\left(\frac{60f\pi}{181}\right)\right]}{G_{91}^{(f)} - G_{89}^{(f)} - 2}\right)\varpi_{40,x}^{(f)}$$

and $\varpi_{40,x}^{(f)}$ and $G_g^{(f)}$ are given in Eqs. (41) and (42), respectively. The 3D view is shown in Fig. 5.

Case 3. When the current J enters from node $d_1(x_1, y_1)$ to node $d_2(x_2, y_1)$, in other words, $y_1 = y_2$. From formula (1), the potential of any node $d(x, y)$ can be written as

$$\frac{U_{u\times v}(x, y)}{J} = \frac{4r_b}{2u+1}\sum_{f=1}^{u}\mathcal{J}_f,$$

where

$$\mathcal{J}_f = \left(\frac{K_{y_1,f}K_{y,f}}{G_{v+1}^{(f)} - G_{v-1}^{(f)} - 2}\right)(\varpi_{x_1,x}^{(f)} + \varpi_{x_2,x}^{(f)}),$$

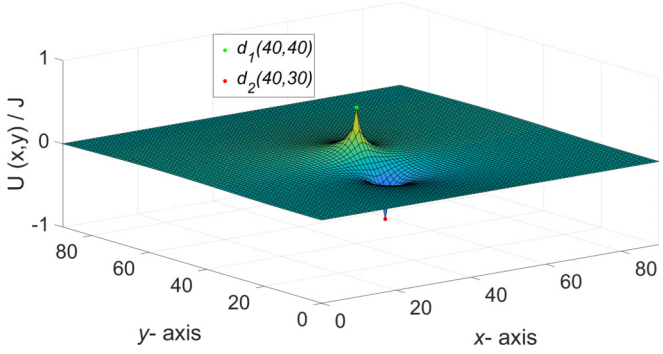

FIG. 5. 3D view for the $U_{90\times90}(x, y)/J$ in Eq. (43).

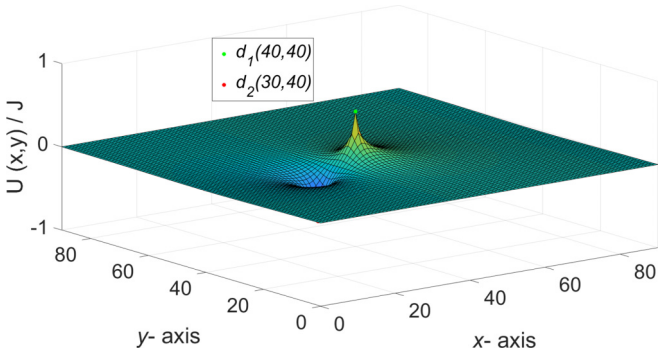

FIG. 6. 3D view for the $U_{90\times90}(x, y)/J$ in Eq. (44).

and $\varpi_{x_m,x}^{(f)}$, $G_g^{(f)}$, and $K_{q,f}$ are defined in Eqs. (2), (3), and (4), respectively.

When $u = v = 90$, $x_1 = y_1 = y_2 = 40$, $x_2 = 30$, and $r_a = r_b = 1$, the following formula is obtained:

$$\frac{U_{90\times90}(x, y)}{J} = \frac{4}{181}\sum_{f=1}^{90}\mathcal{K}_f, \tag{44}$$

where

$$\mathcal{K}_f = \left(\frac{\cos\left(\frac{80f\pi}{181}\right)\sin\frac{2yf\pi}{181}}{G_{91}^{(f)} - G_{89}^{(f)} - 2}\right)(\varpi_{40,x}^{(f)} + \varpi_{30,x}^{(f)}),$$
$$\varpi_{30,x}^{(f)} = (G_{90-|30-x|}^{(f)} + G_{|30-x|}^{(f)}), \tag{45}$$

and $\varpi_{40,x}^{(f)}$ and $G_g^{(f)}(g = 90 - |40 - x|, |40 - x|, 90 - |30 - x|, |30 - x|, 91, 89)$ are given by Eqs. (41) and (42), respectively. The effective resistance is shown in Fig. 6.

Case 4. Presuming that $d_h(x_h, y_1)(h = 1, 2, \ldots, s)$ enters the node at the same latitude as J/s and the current flows out from $O(0, 0)$ as J, the potential formula is obtained:

$$\frac{U(x, y)}{J} = \frac{4r_b}{2u+1}\sum_{f=1}^{u}\mathcal{L}_f,$$

where

$$\mathcal{L}_f = \frac{K_{y_1,j}K_{y,j}}{G_{v+1}^{(f)} - G_{v-1}^{(f)} - 2}\left(\frac{1}{s}\sum_{h=1}^{s}\varpi_{x_h,x}^{(f)}\right),$$

$\varpi_{x_h,x}^{(f)}$ is given by Eq. (2), and $G_g^{(f)}$ and $K_{q,f}$ are the same as Eqs. (3) and (4), respectively.

When $h = 1, 2, 3$, $s = 3$, $u = v = 90$, $x_1 = 50$, $x_2 = 40$, $x_3 = 30$, $y_1 = y_2 = y_3 = 30$, and $r_a = r_b = 1$, the following formula is deduced:

$$\frac{U_{90\times90}(x, y)}{J} = \frac{4}{181}\sum_{f=1}^{90}\mathcal{M}_f, \tag{46}$$

where

$$\mathcal{M}_f = \frac{\sin\left(\frac{80f\pi}{181}\right)\sin\left(\frac{2yf\pi}{181}\right)}{G_{91}^{(f)} - G_{89}^{(f)} - 2}\left(\frac{1}{3}(\varpi_{50,x}^{(f)} + \varpi_{40,x}^{(f)} + \varpi_{30,x}^{(f)})\right),$$
$$\varpi_{50,x}^{(f)} = (G_{90-|50-x|}^{(f)} + G_{|50-x|}^{(f)}).$$

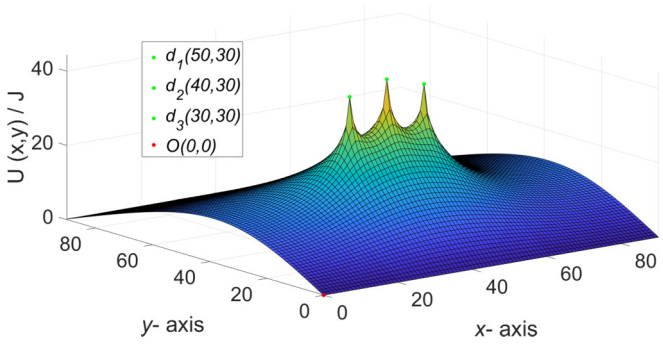

FIG. 7. 3D view for the $U_{90\times90}(x,y)/J$ in Eq. (46).

$\varpi^{(f)}_{40,x}$, $\varpi^{(f)}_{30,x}$ and $G^{(f)}_g(g = 90-|50-x|,\ |50-x|,\ 90-|40-x|,\ |40-x|,\ 90-|30-x|,\ |30-x|,\ 91,\ 89)$ are given by Eqs. (41), (45), and (42), respectively. The 3D view is shown in Fig. 7.

Case 5. At the same time, the effective resistance from $d_1(x_1,y_1)$ to $d_2(x_2,y_2)$ can also be gained,

$$R_{u\times v}(d_1,d_2)=\frac{4r_b}{2n+1}\sum_{f=1}^{u}\mathcal{N}_f, \tag{47}$$

where

$$\mathcal{N}_f=\left(\frac{G^{(f)}_v\left(K^2_{y_1,f}+K^2_{y_2,f}\right)-2\varpi^{(f)}_{x_2,x_1}K_{y_1,f}K_{y_2,f}}{G^{(f)}_{v+1}-G^{(f)}_{v-1}-2}\right),$$

and $\varpi^{(f)}_{x_1,x}$, $G^{(f)}_g$, and $K_{q,f}$ are defined in Eqs. (2), (3), and (4), respectively.

In the scale of $u\times v(90\times90)$, we take y_1 and y_2 as variables. When the coordinate $x_1=x_2=80$ and $r_a=r_b=1$, the following formula is deduced:

$$R_{90\times90}(d_1,d_2)=\frac{4}{181}\sum_{f=1}^{90}\mathcal{O}_f, \tag{48}$$

where

$$\mathcal{O}_f=\left(\frac{G^{(f)}_{90}\left(K^2_{y_1,f}+K^2_{y_2,f}\right)-2\varpi^{(f)}_{80,80}K_{y_1,f}K_{y_2,f}}{G^{(f)}_{91}-G^{(f)}_{89}-2}\right)$$

and $\varpi^{(f)}_{80,80}=G^{(f)}_{90}+G^{(f)}_0$, $G^{(f)}_g(g=90,0,91,89)$ is given by Eq. (42). The 3D view is shown in Fig. 8.

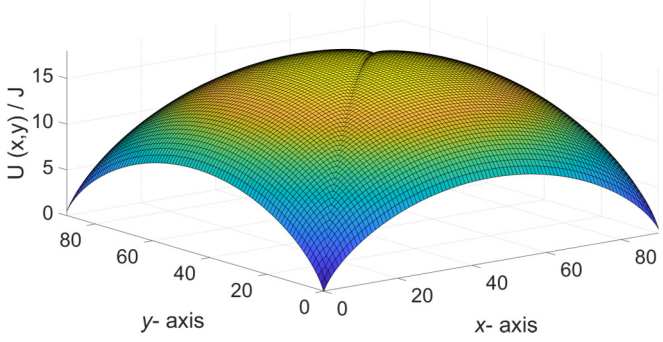

FIG. 8. 3D view for the $U_{90\times90}(x,y)/J$ in Eq. (48).

Proof of Eq. (47). Presuming the potentials at nodes of $d_1(x_1,y_1)$ and $d_2(x_2,y_2)$ are U_1 and U_2, using Ohm's law yields

$$R_{u\times v}(d_1,d_2)=\frac{1}{J}(U_1-U_2). \tag{49}$$

Replacing $(x,y)=(x_1,y_1)$ and $(x,y)=(x_2,y_2)$ into Eq. (1), the following formula is obtained:

$$\frac{U_1}{J}=\frac{U_{u\times v}(x,y)}{J}=\frac{4r_b}{2u+1}\sum_{f=1}^{u}\mathcal{P}_f, \tag{50}$$

where

$$\mathcal{P}_f=\left(\frac{\varpi^{(f)}_{x_1,x_1}K_{y_1,f}-\varpi^{(f)}_{x_2,x_1}K_{y_2,f}}{G^{(f)}_{v+1}-G^{(f)}_{v-1}-2}\right)K_{y_1,f},$$

$\varpi^{(f)}_{x_1,x}$, $G^{(f)}_g$, and $K_{q,f}$ are defined in Eqs. (2), (3), and (4), respectively,

$$\frac{U_2}{J}=\frac{U_{u\times v}(x,y)}{J}=\frac{4r_b}{2u+1}\sum_{f=1}^{u}\mathcal{Q}_f, \tag{51}$$

where

$$\mathcal{Q}_f=\left(\frac{\varpi^{(f)}_{x_1,x_2}K_{y_1,f}-\varpi^{(f)}_{x_2,x_2}K_{y_2,f}}{G^{(f)}_{v+1}-G^{(f)}_{v-1}-2}\right)K_{y_2,f},$$

and $\varpi^{(f)}_{x_m,x}$, $G^{(f)}_g$, and $K_{q,f}$ are defined in Eqs. (2), (3), and (4), respectively. Placing Eqs. (50) and (51) into Eq. (49) gains Eq. (47), where $K_{q,f}$ is defined in Eq. (4).

Case 6. Assuming that the current J goes from $d_1(x_1,y_1)$ to the two output nodes of $d_2(x_2,y_2)$ and $d_3(x_3,y_3)$, where two output currents are respectively $J/2$, this situation is regarded as two independent current sources. From formula (1), the potential formula of an arbitrary node $d(x,y)$ in the horn torus network can be written as

$$\frac{U(x,y)}{J}=\frac{2r_b}{2u+1}\sum_{f=1}^{u}\mathcal{R}_fK_{y,f},$$

where

$$\mathcal{R}_f=\left(\frac{2\varpi^{(f)}_{x_1,x}K_{y_1,f}-\varpi^{(f)}_{x_2,x}K_{y_2,f}-\varpi^{(f)}_{x_3,x}K_{y_3,f}}{G^{(f)}_{v+1}-G^{(f)}_{v-1}-2}\right),$$

$\varpi^{(f)}_{x_m,x}$ is given by Eq. (2) with $m=1,2,3$. The $G^{(f)}_g$ and $K_{q,f}$ are the same as Eqs. (3) and (4), respectively.

When $u=v=90$, $x_1=60$, $x_2=y_1=40$, $y_2=30$, $x_3=y_3=20$, and $r_a=r_b=1$, the following formula is deduced:

$$\frac{U_{90\times90}(x,y)}{J}=\frac{2}{181}\sum_{f=1}^{90}\mathcal{S}_f\sin\frac{2yf\pi}{181}, \tag{52}$$

where

$$\mathcal{S}_f=\left(\frac{2\varpi^{(f)}_{60,x}\sin\frac{80f\pi}{181}-\varpi^{(f)}_{40,x}\sin\frac{60f\pi}{181}-\varpi^{(f)}_{20,x}\sin\frac{40f\pi}{181}}{G^{(f)}_{91}-G^{(f)}_{89}-2}\right),$$

$\varpi^{(f)}_{x_m,x}=G^{(f)}_{v-|x_m-x|}+G^{(f)}_{|x_m-x|}$, $m=1,2,3$, $G^{(f)}_g$ is given by Eq. (42), and $g=90-|60-x|,|60-x|,\ 90-|40-$

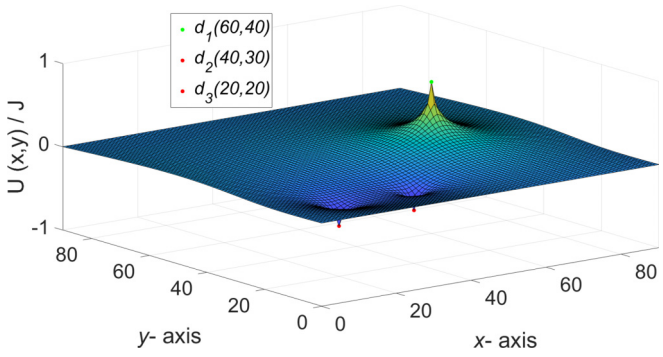

FIG. 9. 3D view for the $U_{90\times90}(x, y)/J$ in Eq. (52).

$x|, |40 - x|, \ 90 - |20 - x|, |20 - x|, \ 91, \ 89$. The 3D view is shown in Fig. 9.

Case 7. When $x_1 = x_2 = 0$, we can get the potential formula of node $(0, 0)$ and node (x, y) as follows:

$$\frac{U_{u\times v}(x, y)}{J} = \frac{4r_b}{2u+1}\sum_{f=1}^{u}\mathcal{T}_f K_{y,f},$$

where

$$\mathcal{T}_f = \left(\frac{\varpi^{(f)}_{x_1,x}K_{y_1,f} - \varpi^{(f)}_{x_2,x}K_{y_2,f}}{G^{(f)}_{v+1} - G^{(f)}_{v-1} - 2}\right),$$

and $\varpi^{(f)}_{x_m,x}$, $G^{(f)}_g$, and $K_{q,f}$ are defined in Eqs. (2), (3), and (4), respectively.

When $u = v = 90, \ x_1 = y_1 = y_2 = 40, \ x_2 = 0$, and $r_a = 1, \ r_b = 90$, we can get

$$\frac{U_{90\times90}(x, y)}{J} = \frac{360}{181}\sum_{f=1}^{90}\mathcal{U}_f, \tag{53}$$

where

$$\mathcal{U}_f = \left(\frac{\varpi^{(f)}_{40,x}K_{40,f} - \varpi^{(f)}_{0,x}\sin\frac{80f\pi}{181}}{G^{(f)}_{91} - G^{(f)}_{89} - 2}\right)\sin\frac{2fy\pi}{181},$$

$$\varpi^{(f)}_{0,x} = G^{(f)}_{90-|-x|} + G^{(f)}_{|-x|},$$

$\varpi^{(f)}_{40,x}$, $G^{(f)}_g$ are given by Eqs. (41) and (42), and $g = 90 - |40 - x|, |40 - x|, \ 90 - x, \ x, \ 91, \ 89$. The 3D view is shown in Fig. 10.

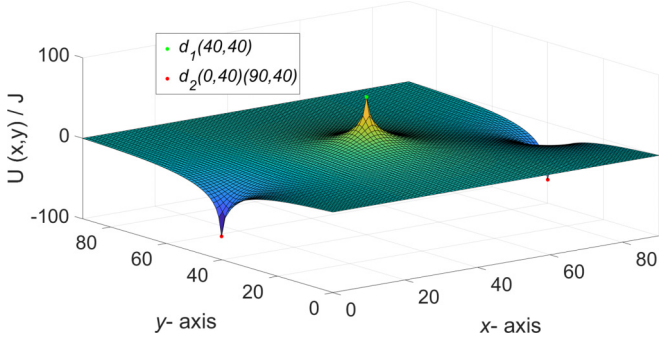

FIG. 10. 3D view for the $U_{90\times90}(x, y)/J$ in Eq. (53).

V. FAST NUMERICAL ALGORITHM FOR COMPUTING $U_{u\times v}(x, y)/J$

In order to realize fast calculation of the potential for large-scale resistor networks, in this section, by summarizing the previous discussion and analysis, we give a fast numerical algorithm of the potential by Eqs. (3), (5), (7), (9), (10), (11), (24), (25), and (35) and the famous fifth kind of discrete sine transform (DST-V).

Algorithm 1 Fast matrix-vector multiplication $\mathbf{Q}_u\mathbf{v} = \mathbf{y}$

Step 1. Compute y_1 by the equation
$y_1 = (2 + 2\sigma)v_1 - \sigma v_2$;
Step 2. Cycle computing y_i by the equation
$y_i = (-\sigma)v_{i-1} + (2 + 2\sigma)v_i - \sigma v_{i+1}$,
$i = 2, \ldots, u - 1$;
Step 3. Compute y_u by the equation
$y_u = (-\sigma)v_{u-1} + (2 + 3\sigma)v_u$.

Algorithm 2 Fast algorithm for computing $U_{u\times v}(x, y)/J$

Step 1. Compute ι_f by Eq. (5), $f = 1, 2, \ldots, u$;
Step 2. Compute
$\cosh\varphi_f = \frac{\iota_f}{2}$, $f = 1, 2, \ldots, u$;
Step 3. Compute $G^{(f)}_g$ by Eq. (3),
$g = v - |x_t - x|, \ |x_t - x|, \ v + 1, \ v - 1$,
$t = 1, 2, \ \ f = 1, 2, \ldots, u$;
Step 4. Compute $R^{(f)}_x$ by Eq. (35),
$x = 0, 1; \ f = 1, 2, \ldots, u$;
Step 5. Compute V_g by Eqs. (24), (25), and
DST-V, $g = 0, 1$;
Step 6. Compute Q_uV_g by the algorithm 1,
$g = 1, 2, \ldots$;
Step 7. Cycle computing V_g by Eqs. (9), (10),
and (11), $g = 2, 3, \ldots$;
Step 8. Compute $U_{u\times v}(x, y)/J$ by Eq. (7).

The general idea of a fast numerical algorithm is as follows: $\mathbf{R}_0$ and $\mathbf{R}_1$ can be obtained through Eq. (35); $\mathbf{V}_0$ and $\mathbf{V}_1$ can be obtained by the $\mathbf{V}_g = \mathbf{S}^V_u\mathbf{R}_g$, $\mathbf{R}_0$, and $\mathbf{R}_1$; $\mathbf{V}_2$ can be calculated by Eq. (9), fast matrix-vector multiplication, $\mathbf{V}_0$ and $\mathbf{V}_1$; and so on.

As is well known, the complexity of tridiagonal matrix-vector multiplication is $O(n)$, which is the same as Algorithm 1. Moreover, one DST-V needs $2n\log_2 n + O(n)$ real arithmetic operations [56,57]. So the complexity of Algorithm 2 is $4n\log_2 n + O(n)$, which consists of two DST-V and Algorithm 1. According to the above two algorithms, two examples are used to vividly show the iterative effect of large-scale data.

Example 1. In the network with $u = 300$ and $v = 10$, the current flows in from $(x_1, y_1)(x_1 = 2, y_1 = 200)$ and out from $(x_2, y_2)(x_2 = 8, y_2 = 80)$. Let $r_b = 1$, $r_a = 100$, and $J = 1$. According to the results of computing $U_{300\times10}(x, y)/J$ by Algorithm 2, we can get a 3D graph (Fig. 11).

Example 2. In the scale of $u \times v(1000 \times 10)$, when the current $x_1 = 2, \ x_2 = 8, \ y_1 = 700, \ y_2 = 400, \ r_b = 1, r_a = 100$, and $J = 1$. The results of computing $U_{1000\times10}(x, y)/J$ by Algorithm 2 are shown in Fig. 12.

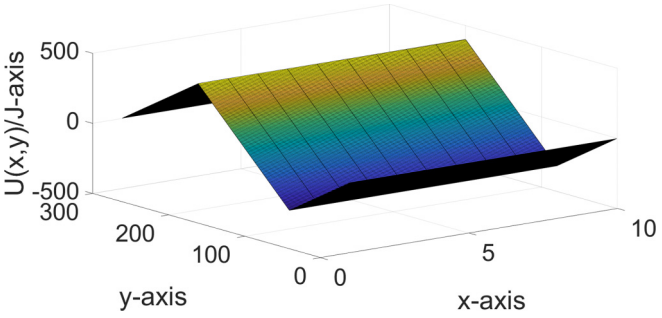

FIG. 11. 3D graph for the changes of $U_{300\times10}(x, y)/J$ with x and y.

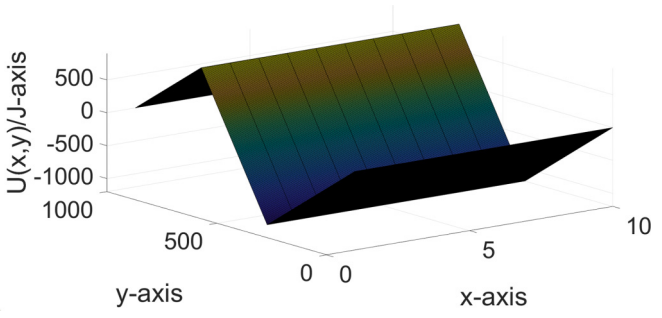

FIG. 12. A 3D graph for the changes of $U_{1000\times10}(x, y)/J$ with x and y.

VI. CONCLUSIONS

The main innovation of this paper is to derive a resistor network model, i.e., the horn torus resistor network model, based on which an exact potential formula and a fast algorithm are proposed. The process of forming a 3D dynamic view for some interesting potential functions are vividly displayed. This makes the calculation of the resistor network not only limited to manual calculation, but also realized for fast calculation of potential for large-scale resistor networks. The horn torus-resistor network provides a network model and tool for many fields such as natural science. It provides substantial development for promoting the diversity of resistor network models. Horn torus networks often appear in the research of astronomy and cosmology, as well as in the "Topological spin exceptions on a rigid torus" [58]. It is expected that the research ideas and methods in this paper can also be used to study relevant scientific problems in the above fields. In addition, by using the idea and method of the studying resistor network, it would interesting to study the recurrent neural network [16–22]. That will be our next step.

ACKNOWLEDGMENTS

The research was supported by the Natural Science Foundation of Shandong Province (Grant No. ZR2022MA092) and the National Natural Science Foundation of China (Grants No. 12101284 and No. 12001257).

[1] Y. Hadad, J. C. Soric, A. B. Khanikaev, and A. Alù, Nat. Electron. **1**, 178 (2018).
[2] D. Zhang, B. Yang, J. Tan, Y. Jin, B. Xiao, G. Xian, X. Xue, and Y. Li, Compos. Struct. **276**, 114587 (2021).
[3] G. Kirchhoff, Ann. Phys. Chem. **148**, 497 (1847).
[4] G. Ferri and G. Antonini, J. Circuit Syst. Comp. **16**, 489 (2007).
[5] M. Owaidat, R. Hijjawi, and J. Khalifeh, Int. J. Theor. Phys. **51**, 3152 (2012).
[6] S. Katsura and S. Inawashiro, J. Math. Phys. **12**, 1622 (1971).
[7] C. Pennetta, E. Alfinito, L. Reggiani, F. Fantini, I. DeMunari, and A. Scorzoni, Phys. Rev. B **70**, 174305 (2004).
[8] W. Kook, Adv. Appl. Math. **46**, 417 (2011).
[9] J. Cserti, Am. J. Phys. **68**, 896 (2000).
[10] F. Wu, J. Phys. A: Math. Gen. **37**, 6653 (2004).
[11] W. Tzeng and F. Wu, J. Phys. A: Math. Gen. **39**, 8579 (2006).
[12] N. S. Izmailian and M.-C. Huang, Phys. Rev. E **82**, 011125 (2010).
[13] N. S. Izmailian, R. Kenna, and F. Wu, J. Phys. A: Math. Theor. **47**, 035003 (2014).
[14] N. S. Izmailian and R. Kenna, Chin. J. Phys. **53**, 88 (2015).
[15] N. Chair, Ann. Phys. (NY) **341**, 56 (2014).
[16] Y. Shi, L. Jin, S. Li, J. Li, J. Qiang, and D. K. Gerontitis, IEEE Trans. Neural Netw. Learning Syst. **33**, 587 (2022).
[17] Y. Shi, W. Zhao, S. Li, B. Li, and X. Sun, IEEE Trans. Neural Netw. Learning Syst. (unpublished), doi: 10.1109/TNNLS.2021.3108050.
[18] K.-P. Liu, Y. Liu, Y. Zhang, L. Wei, Z. Sun, and L. Jin, Eng. Appl. Artific. Intell. **103**, 104306 (2021).
[19] Z.-B. Sun, G. Wang, L. Jin, C. Cheng, B. Zhang, and J. Yu, Expert Syst. Appl. **192**, 116272 (2022).
[20] L. Jin, Y. Qi, X. Luo, S. Li, and M. Shang, IEEE Trans. Automat. Sci. Eng. **19**, 3575 (2022).
[21] L. Jin, Y. Zhang, S. Li, and Y. Zhang, IEEE Trans. Ind. Electron. **63**, 6978 (2016).
[22] L. Jin, X. Zheng, and X. Luo, IEEE/CAA J. Autom. Sin. **9**, 854 (2022).
[23] Z.-Z. Tan, *Resistor Network Model* (Xiandian University Press, Xi'an, 2011).
[24] Z.-Z. Tan, Chin. Phys. B **26**, 090503 (2017).
[25] Z. Tan, Z.-Z. Tan, and J. Chen, Sci. Rep. **8**, 15601 (2018).
[26] J.-Y. Wu, L. Wang, L.-Y. Ding, and Z.-Z. Tan, Phys. Scr. **94**, 105818 (2019).
[27] Z.-Z. Tan and Z. Tan, Acta Phys. Sin. **69**, 020502 (2020).
[28] Z.-Z. Tan, Eur. Phys. J. Plus **137**, 546 (2022).
[29] Z.-Z. Tan and Z. Tan, Phys. Scr. **95**, 035226 (2020).
[30] H.-X. Chen and Z.-Z. Tan, Phys. Scr. **95**, 085204 (2020).
[31] Z.-Z. Tan and Z. Tan, Commun. Theor. Phys. **72**, 055001 (2020).
[32] Z.-Z. Tan and Z. Tan, Chin. Phys. B **29**, 080503 (2020).
[33] H.-X. Chen, M.-Y. Wang, W.-J. Chen, X.-Y. Fang, and Z.-Z. Tan, Phys. Scr. **96**, 075202 (2021).
[34] Y.-R. Fu, X. Jiang, Z. Jiang, and S. Jhang, Comput. Appl. Math. **39**, 146 (2020).
[35] Y.-R. Fu, X. Jiang, Z. Jiang, and S. Jhang, J. Appl. Anal. Comput. **10**, 1599 (2020).
[36] L. Du, T. Sogabe, and S.-L. Zhang, Appl. Math. Lett. **75**, 74 (2018).

[37] Y.-L. Wei, Y.-P. Zheng, Z. Jiang, and S. Shon, J. Appl. Math. Comput. **68**, 623 (2022).
[38] Y.-L. Wei, X. Jiang, Z. Jiang, and S. Shon, J. Appl. Anal. Comput. **10**, 178 (2020).
[39] J.-T. Jia, Numer. Algorithms **83**, 149 (2020).
[40] Y.-J. Zhou and Z.-D. Luo, Adv. Diff. Eq. **2019**, 1 (2019).
[41] Z.-Z. Tan, Chin. Phys. B **24**, 020503 (2015).
[42] Z.-Z. Tan, Phys. Rev. E **91**, 052122 (2015).
[43] Z.-Z. Tan, Sci. Rep. **5**, 11266 (2015).
[44] Z.-Z. Tan, J. W. Essam, and F. Y. Wu, Phys. Rev. E **90**, 012130 (2014).
[45] J. W. Essam, Z.-Z. Tan, and F. Y. Wu, Phys. Rev. E **90**, 032130 (2014).
[46] Z.-Z. Tan and J.-H. Fang, Commun. Theor. Phys. **63**, 36 (2015).
[47] Z.-Z. Tan, Int. J. Circ. Theor. Appl. **43**, 1687 (2015).
[48] Z.-Z. Tan, Commun. Theor. Phys. **67**, 280 (2017).
[49] Z.-Z. Tan, Chin. Phys. B **25**, 050504 (2016).
[50] Z. Tan, Z.-Z. Tan, and J. Chen, Sci. Rep. **8**, 5798 (2018).
[51] Z. Tan and Z.-Z. Tan, Sci. Rep. **8**, 9937 (2018).
[52] G. Udrea, Port. Math. **53**, 143 (1996).
[53] J. C. Mason and D. C. Handscomb, *Chebyshev Polynomials* (Chapman and Hall/CRC, London, 2002).
[54] S. R. Garcia and S. Yih, Commun. Alg. **46**, 3745 (2018).
[55] V. Sanchez, P. Garcia, A. M. Peinado, J. C. Segura, and A. J. Rubio, IEEE Trans. Signal Process. **43**, 2631 (1995).
[56] Y. Liu and C.-Q. Gu, Appl. Math. Comput. **349**, 1 (2019).
[57] P. Yip and K. Rao, in *ICASSP'85. IEEE International Conference on Acoustics, Speech, and Signal Processing* (IEEE, New York, 1985), Vol. 10, pp. 776–779.
[58] V. L. Carvalho-Santos, A. R. Moura, W. A. Moura-Melo, and A. R. Pereira, Phys. Rev. B **77**, 134450 (2008).